Indian Journal of Chemistry
Vol. 63, November 2024, pp. 1083-1095
DOI: 10.56042/ijc.v63i11.10788

(E)-3-(4-Hydroxyphenyl)-1-(4-methoxyphenyl)prop-2-en-1-one: DFT/TD-DFT-based investigations with distinct solvents and *in silico* ADME profiling

Sümeyya Serin
Inonu University, Scientific and Technological Research Center, 44280, Malatya, Turkey
E-mail: sumeyya.alatas@inonu.edu.tr

Received 29 April 2024; accepted (revised) 22 October 2024

The chalcone scaffold has become one of the privileged structures frequently encountered in medicinal chemistry for the discovery of new and effective drug candidates. In recent years, chalcone derivatives have attracted intense attention from both experimental and theoretical researchers due to their ease of synthesis and wide range of biological activities. Herein, quantum chemical-based calculations have been performed on chalcone derivative (E)-3-(4-hydroxyphenyl)-1-(4-methoxyphenyl)prop-2-en-1-one. Density functional theory (DFT) method has been applied with the B3LYP hybrid functional and 6-311++G (d, p) basis set. The structural, electronic, energetic and reactivity properties of the mentioned chalcone derivative have been examined. Bond parameters and vibrational analysis results are compatible with experimental data. The energy gap (ΔE) values corresponding to acetonitrile, DMSO and water phases have been calculated as 3.753, 3.750 and 3.747 eV, respectively. Also, the reactive regions of the molecule have been visualized with molecular electrostatic potential (MEP) maps. The excited state characteristics of the title compound in water, acetonitrile and DMSO environments have been calculated by the TD-DFT method. All absorption wavelengths could be qualified as π→π* and n→π* transition type. A bioavailability radar has been created by calculating some physicochemical parameters such as lipophilicity, TPSA, and water solubility. ADME properties have been predicted from pharmacokinetics and drug likeness data.

Keywords: Chalcone, DFT, Solvent effect, NBO, ADME profiling

Chalcones are open-chain all-purpose molecules consisting of three-carbon, unsaturated carbonyl system connecting two aromatic rings. It serves as a precursor for the biosynthesis of flavonoids and isoflavonoids and forms the core infrastructure for many hybrid substances[1,2]. At the same time, chalcone-derived compounds have become the focus of attention in many pharmacological fields due to their bioactive nature. Activities such as anticancer[3], antihypertensive[4], antioxidant[5], anti-inflammatory[6,7], anticonvulsant[8], antibacterial[9], and antifungal[10] can be given as examples of the pharmacological applications they exhibit. In addition, with potential applications in different disciplines appearing in the literature, studies on the design, synthesis and determination of application areas of more specific chalcone derivatives have gained momentum[11]. In the literature, it is possible to find dozens of studies conducted in this field in recent years. Some of the selected studies are summarized in Table 1 along with their outlines[12-20]. Responses to questions regarding the recent advances on this topic were described in Table 1. As highlighted in Table 1, the principal motivation for the synthesis of new derivatives containing chalcone core is that they have clinical potential against a wide range of diseases. Also, the ease of synthesis provides an additional advantage. However, the development of effective synthesis strategies, isolation of new variants, target identification, and elucidation of mechanisms of action remain a challenging process[21]. In such cases, computational chemistry methods and *in silico* screening studies offer researchers new and effective perspectives. With this respect, predicting the structural, electronic, energetic, and physicochemical characteristics of new derivatives by applying structural optimization at the design stage is a frequently preferred effective strategy. On the other hand, *in silico* profiling provides insight into research on target identification, determination of bioactivity and mechanisms of action. For instance, in order to get insights into oral bioavailability in the development of bioactive candidates, estimating many more determining factors of the relevant molecules

Table 1 — Several recent studies on the synthesis and applications of chalcone derivatives

Ref.	Target	Process	Key Findings
12	*Synthesis and characterization of chalcone ligated molybdenum carbonyl complexes *Investigation of cytotoxicity and binding abilities to quadruplex DNA	*Microwave-assisted synthesis *X-ray crystallographic studies *Brine shrimp lethality assay *Fluorescence intercalator displacement (FID) assay	Molybdenum complexes of pyridine carboxaldehydes, acetylpyridines and pyridyl-antryl chalcones were synthesized. It was concluded that the cytotoxicity and DNA binding abilities of molybdenum carbonyl compounds improved by adding a chalcone derivative to the structure.
13	*Investigation of anti-inflammatory activities of previously synthesized naphthalene-chalcone hybrids	*Carrageenan-induced rat paw edema method *Molecular docking study **In silico* ADME analysis	It was determined that *ortho* and *para* difluoro substituted chalcone derivative showed crucial anti-inflammatory activity in carrageenan-induced rat paw edema method. In-Silico ADME studies revealed that all compounds demonstrated acceptable pharmacokinetic properties.
14	*Synthesis of new chromene-chalcone and chromene-pyrazole hybrid molecules *Investigation of cytotoxicity	**In vitro* anticancer activity **In silico* ADMET analysis	Among the synthesized compounds, 4-fluorophenyl pyrazole substituted and naphthyl pyrazole substituted derivatives were determined to exhibit significant anticancer activity against MDA-MB-231 and MCF-7 cells.
15	*Synthesis of new 1,2,3-triazole-tethered chalcone derivatives *Investigation of anti-inflammatory and antioxidant activity	*The click chemistry approach *% Inhibition of hemolysis activity * DPPH anti-oxidant activity *Molecular docking study **In silico* ADME analysis	It was determined that many of the derivatives synthesized and characterized by spectroscopic methods showed anti-inflammatory and antioxidant activities. Also, the results were supported by molecular modeling studies.
16	*Synthesis of 25 push–pull type chalcone derivatives by modifying the chalcone skeleton *Examination of optical and electrochemical properties	*Photophysical properties in $CHCl_3$ *Solid-state photophysical properties *Electrochemical studies *DFT study	Outcomes obtained from the photophysical and electronic features of push–pull chalcone present the possibility of adaptively tuning the optical and electronic features of chalcone in both $CHCl_3$ solution and solid state. DFT techniques were utilized to determine the structure and electronic properties, including E_{HOMO}&E_{LUMO} and other quantum chemical descriptors.
17	*Investigation of the effectiveness of previously synthesized nitrogen-based chalcone analogs on KRAS mutant CRC	*Cell culture *Cell viability assay *Morphological examination *Colony formation *Flow cytometric analysis of cell cycle *Invasion assay *Western blot analysis *Statistical analysis	Tests and analyzes performed within the scope of the study revealed that mentioned chalcone compounds may be effective in the treatment of human CRC, especially KRAS mutant CRC, as well as other types of cancer.
18	*Synthesis of thienyl chalcones using iron oxide nanoparticles (FeONPs) as a heterogeneous catalyst	*Sonochemical method *X-ray diffraction (XRD) pattern	A new and effective method using sonochemistry to synthesize thienyl chalcones has been developed (high yields of up to 94%).
19	*Design and synthesis of chalcone derivatives containing benzoxazole	*Anti-bacterial activity test **In vivo* inhibitory activity **In vivo* antiviral activity assay *Molecular docking study	Biological analyzes showed that some of the synthesized derivatives exhibited excellent antibacterial and antiviral activities. In conclusion, this study reveals the applicability of chalcone derivatives in pesticides.
20	*Design and synthesis of a novel series of cycloheptapyridinone fused 1,2,3–triazolyl chalcones *Creation of new methods to modify compounds with a 1,2,3–triazole and chalcone scaffolds	*Antimicrobial and antifungal activity **In vitro* antitubercular effect *Molecular docking study **In silico* ADMET prediction	Synthesis of aimed chalcone derivatives was carried out by utilizing the Claisen–Schmidt functionalized carbonyl coupling reaction. According to bioactivity tests, dichloro, difluoro and OH-substituted hybrids exhibited exceptional antibacterial activities with zone of inhibition 27, 32, and 38 mm against the tested E. faecalis bacteria, whereas difluoro substituted derivative displayed better antitubercular potency against M. tuberculosis H37Rv strain with MIC value 5.25 µg/mL

such as lipophilicity, polar surface area, and numbers of hydrogen-bond acceptors and donors, will shed light on studies. Furthermore, it is vital to determine water solubility values in order to accomplish *in vitro* experiments and move on to the *in vivo* phase. Therefore, quantum chemical methods and *in silico* screening have become important tools that offer advanced perspectives to modern drug design studies, enabling researchers to develop candidates with fewer side effects, potent and superior pharmacokinetic properties.

Keeping these considerations in mind, in this current study, the methoxy substituted chalcone derivative synthesized by Qiu *et al.*[22] was subjected to quantum chemical and *in silico* examinations. Cytotoxicity evaluation of the compound in question was performed by Wilhelm et al[23]. As far as we know, no comprehensive theoretical and/or *in silico* study has been found in the literature for the relevant compound. In this context, structural, vibrational, electronic, energetic and physicochemical properties of the title compound were examined by performing DFT-based calculations. Calculations were repeated in three distinct solvent environments (acetonitrile, DMSO, and water) to determine solvent effects. Considering the importance of chalcone derivatives in the field of medicinal chemistry, it was concluded that including *in silico* analyzes in the study would be of great benefit. Therefore, it is expected that the findings of the study will guide and inspire many further studies.

Computational Methodology

All DFT computations represented in this study were performed by using GAUSSIAN 16 software package[24] on applying the B3LYPhybrid functional and the 6-311++G (d, p)split-valence triple zeta basis set to examine the optimized structure of studied chalcone derivative[25-27]. Gauss View 6 software[28] was utilized for visualizations of the optimized structure, FMOs, and MEP diagrams. To gain the density of states (DOS) plot, Gauss-Sum 3.0 program[29] was operated. The solvent phase calculations were carried out by using **I**ntegral **E**quation **F**ormalism **P**olarizable **C**ontinuum **M**odel (IEFPCM) [30,31]. Acetonitrile (ε=35.7), DMSO (*ε*=46.8), and water (*ε*=78.4) environments were simulated by mentioned solvent model. For computations, optimized structure was verified by the absence of imaginary frequency. The TD-DFT method[32-36] was utilized to enlighten UV–vis. features such as possible electronic transitions, energies, and oscillator strengths. To appraise basic physicochemical and lipophilicity features of studied compound, SwissADME web server[37] was utilized. The n-octanol/water partition coefficient ($logP_{ow}$) was established utilizing five methodologies, which were ILOGP, XLOGP3, WLOGP, MLOGP, and SILICOS-IT[38-42]. Additionally, molecular lipophilicity potential (MLP) map of studied compound was visualized in Molinspiration Galaxy 3D Structure Generator v2018.01 beta[43, 44].

The thermochemical quantities, $E_{vib.}$ (vibrational thermal energy), $S_{vib.}$ (vibrational entropy), and $Cv_{vib.}$ (vibrational heat capacity) of the studied molecule were calculated through specific equations ((1)-(5)) defined below in accordance with the principles of quantum mechanics[45-48]. The following explanations refer to the terms presented in the equations:$\Theta_{v,j}=hvj/k$ →vibrational temperature, k→ Boltzmann constant, h→ Planck constant, and vj→ j^{th} fundamental frequency.

$$Q = Q_{trans.} \times Q_{rot.} \times Q_{vib.}Q_{elec.} \quad \text{... (1)}$$

$$Q_{vib.} = \prod_{j=1}^{3N-6} \frac{e^{-\Theta_{v,j}/2T}}{\left(1 - e^{-\frac{\Theta_{v,j}}{T}}\right)} \quad \text{... (2)}$$

$$E_{vib.} = Nk \sum_{j=1}^{3N-6} \left(\frac{\Theta_{v,j}}{2} + \frac{\Theta_{v,j} e^{-\Theta_{v,j}/T}}{\left(1 - e^{-\frac{\Theta_{v,j}}{T}}\right)} \right) \quad \text{... (3)}$$

$$S_{vib.} = Nk \sum_{j=1}^{3N-6} \left[\frac{\Theta_{v,j}/T}{\left(e^{\Theta_{v,j}/T} - 1\right)} - ln\left(1 - e^{-\Theta_{v,j}/T}\right) \right] \quad \text{... (4)}$$

$$Cv_{vib.} = Nk \sum_{j=1}^{3N-6} \left[\left(\frac{\Theta_{v,j}}{T}\right)^2 \frac{e^{\Theta_{v,j}/T}}{\left(e^{\Theta_{v,j}/T} - 1\right)^2} \right] \quad \text{... (5)}$$

According to Koopmans theorem[49], ionization energy (I)($I = -E_{HOMO}$) and electron affinity (A) ($A = -E_{LUMO}$) values can be defined by Highest Occupied Molecular Orbital (HOMO) and Lowest Unoccupied Molecular Orbital (LUMO) energies. Additionally, some DFT-based reactivity parameters, calculated using I and A values, with their corresponding equations are presented below ((6)-(13)) [50-56].

Chemical Potential $$\mu = -\frac{I + A}{2} \quad \text{... (6)}$$

ChemicalHardness $$\eta = \frac{I - A}{2} \quad \text{... (7)}$$

Electronegativity $$\chi = \frac{I + A}{2} \quad \text{... (8)}$$

Electrophilicity Index $$\omega = \frac{\mu^2}{2\eta} \quad \text{... (9)}$$

Electron-Accepting Power $$\omega^+ \approx (I + 3A)^2/(16(I - A)) \quad \text{... (10)}$$

Electron-Donating Power $$\omega^- \approx (3I + A)^2/(16(I - A)) \quad \text{... (11)}$$

Maximum Charge Transfer Capability $$\Delta N_{max} = \frac{I + A}{2(I - A)} \quad \text{... (12)}$$

Back-Donation Energy $$\Delta\varepsilon_{back-donation} = -\frac{\eta}{4} \quad \text{... (13)}$$

NBO analysis were performed utilizing the 2nd-order Fock matrix[57,58] at DFT/B3LYP/6–311++G (d, p) theory level. So, donor-acceptor orbital interactions, hybridization types, and stabilization energy predictions were elucidated. Stabilization energy values were calculated according to the formula specified in equation (14). The terms in the formula are expressed as follows: $E^{(2)}$: Stabilization energy, *qi*: Donor orbital occupancy, *Fij:* Off diagonal Fock matrix, *εi* and *εj*: diagonal element, donor and acceptor orbital energies.

$$E^{(2)} = \Delta E_{ij} = qi\left[\frac{(Fij)^2}{(\varepsilon j - \varepsilon i)}\right] \quad \text{... (14)}$$

Results and Discussion

Molecular structure

The ground-state geometry of the title compound was optimized using DFT/B3LYP/6-311++G (d, p) methodology in the gas phase. The X-Ray structure was employed for optimization[23]. The crystal structure was ensured from the Cambridge Crystallographic Data Centre (CCDC 2062758) [23]. The resulting optimized structure is depicted in Fig. 1(a) along with the numbering and labelling scheme. Also, molecular geometry of the relevant compound determined by XRD was superimposed with the geometry of the DFT-optimized structure and Fig. 1(b) was obtained. The obtained RMSD (root mean square deviation) value of 0.077 Å reflects the suitability of the theoretical model used in the current study. In other words, it is concluded that the difference between experimental and theoretical structures is at an acceptable level.

Some of the experimental[22] and theoretical bond parameters of the title compound are listed in Table 2. Accordingly, while the bond lengths of C5=O1, C11-O2, and C12-O3 were theoretically calculated as

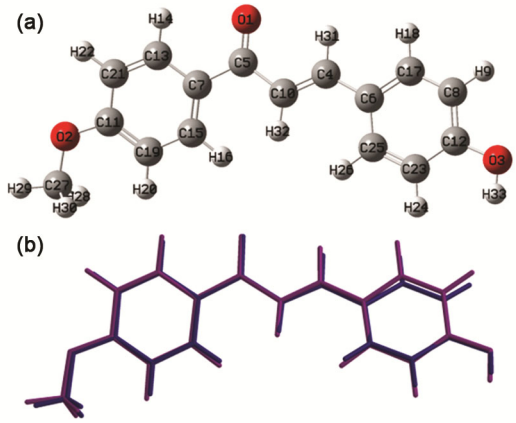

Fig. 1 — DFT-optimized molecular structure of the title compound at B3LYP/6-311++G (d, p) level (a); Atom-by-atom superimposition of the optimized structure (purple) and the X-ray (blue) (b)

Table 2 — Selected bond parameters for title compound

Bond Length (Å)	Exp.	DFT	Bond Length (Å)	Exp.	DFT
C5-O1	1.237	1.227	C7-C15	1.385	1.398
C12-O3	1.361	1.364	C7-C13	1.398	1.407
C11-O2	1.415	1.359	C5-C10	1.463	1.483
C6-C17	1.386	1.407	C5-C7	1.473	1.496
C6-C25	1.398	1.406	C10-C4	1.328	1.346
Bond Angle (°)	Exp.	DFT	Bond Angle (°)	Exp.	DFT
C17-C6-C25	116.87	117.39	O2-C11-C19	125.22	124.56
C17-C6-C4	120.22	118.93	O2-C11-C21	115.27	115.79
C25-C6-C4	122.77	123.66	O3-C12-C8	117.12	117.57
O1-C5-C10	120.40	121.12	O3-C12-C23	123.04	122.59
O1-C5-C7	119.33	119.87	C4-C10-C5	122.63	120.37
Dihedral Angle (°)	Exp.	DFT	Dihedral Angle (°)	Exp.	DFT
O2-C11-C19-C15	179.7	179.9	O3-C12-C8-C17	–179.22	–179.98
C27-O2-C11-C21	–178.6	–179.6	C6-C17-C8-C12	–2.3	–0.1
C7-C5-C10-C4	168.96	176.67	C13-C7-C15-C19	0.3	–0.1
C17-C6-C4-C10	176.0	178.71	C27-O2-C11-C19	0.9	–0.03

1.227, 1.359, and 1.364 Å, they were experimentally reported as 1.237, 1.415, and 1.361 Å, respectively. C-C bond lengths of aromatic rings were theoretically predicted to be in the range of 1.398-1.407 Å, according to X-ray results, these values were determined to be in the range of 1.385-1.398 Å experimentally. On the other hand, bond angles of O1-C5-C10, O1-C5-C7, O2-C11-C19, O2-C11-C21, O3-C12-C8, and O3-C12-C23 were theoretically/(experimentally) determined as 121.12°/(120.40), 119.87°/(119.33), 124.56°/(125.22), 115.79°/(115.27), 117.57°/(117.12) and 122.59°/(123.04), respectively. On comparing the dihedral angles, the values of O2-C11-C19-C15, C27-O2-C11-C21, C7-C5-C10-C4, C17-C6-C4-C10, and O3-C12-C8-C17 angles have been experimentally reported as 179.7°, –178.6°, 168.96°, 176.0°, and –179.22°, respectively. On the other hand, it can be seen from Table 2 that the experimental values of the C6-C17-C8-C12, C13-C7-C15-C19, and C27-O2-C11-C19 angles are determined as –2.3°, 0.3°, and 0.9°, respectively. It is clear that the calculated values of the mentioned dihedral angles are quite close to the experimental values. X-ray and DFT outcomes reveal that the title compound exhibits a nearly planar molecular structure.

Vibrational spectral analysis

The literature survey revealed that neither experimental nor theoretical FT-IR spectral characterization of the studied compound was available.Therefore, in this current study, the theoretical vibrational analysis throughputs of the mentioned molecule were evaluated in a detailed manner. In this respect, the FT-IR spectrum created at the B3LYP/6-311++G (d, p) theory level is exhibited in Fig. 2. Since studied compound consists of 33 atoms, it exhibits total 93 different vibrational modes figured out according to the 3N-6 formula. The selected vibrational mode assignments for the title compound are given in Table 3. The vibrational modes between 3830 cm^{-1} and 1710 cm^{-1} were scaled by 0.983, and modes between 1655 cm^{-1} and 848 cm^{-1} were scaled by 0.958[59].

The characteristic vibrational wavenumber regions of C–H stretching vibrations are in the range of 3100-3000 cm^{-1} [60]. The theoretical C-H symmetric stretching vibrations of title compound appeared at 3153, 3148, 3143, 3142, 3132 and 3092 cm^{-1} as pure bonding vibration with lower IR intensities.Similarly, C-H asymmetric stretching vibrations were detected in the 3131, 3125, 3116, and 3096 cm^{-1} regions.On the other hand, symmetric and asymmetric stretching vibrations belonging to the methoxy group were determined in regions of 2957 cm^{-1} and 3084/3017 cm^{-1}, respectively.Also, CH_3 symmetric bending umbrella mode was computed as the pure mode at 1413 cm^{-1} region.In general, hydroxyl stretching vibrations (νOH) cause bands around 3500-3700 cm^{-1} [61]. In title compound, the computed O-H stretching wavenumber was assigned at 3765 cm^{-1} as a pure mode.The strongest peaks of the simulated FT-IR spectrum are observed at 1572, 1557, and 1135 cm^{-1} with IR intensities of 394, 608, and 542 km/mol, respectively.The peaks in the region of 1572 and 1557 cm^{-1} have been attributed νC=O stretching vibration, in addition, νC=O vibration modes are combined with νCC and ipb HCC modes.The same vibrations were also identified at 1681 and 1585 cm^{-1}.νC–O modes for the title compound were determined at 1235, 1225, 1015, and 991 cm^{-1}.

Thermodynamic parameters

The thermodynamic parameters of title compound were calculated using B3LYP functional with 6-

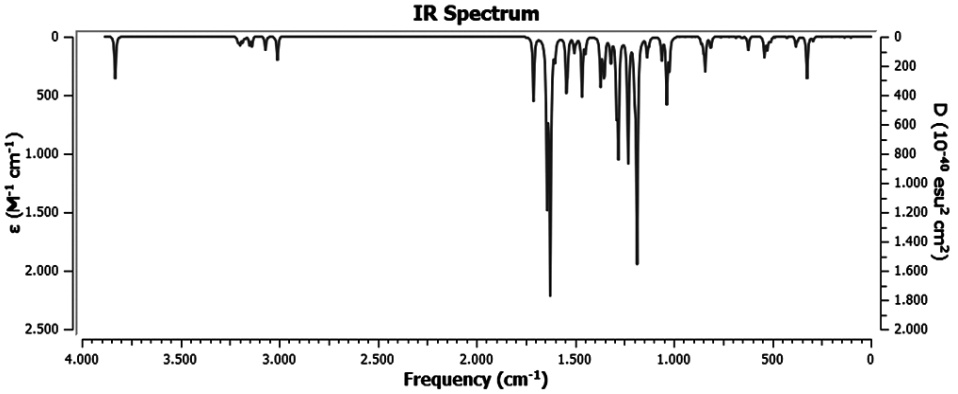

Fig. 2 — Theoretically simulated FT-IR spectrum of title compound

Table 3 — The computed approximate frequencies (in cm^{-1}) for title compound

Assignment	I_{IR}	Unscaled	Scaled
νOH	104	3830	3765
νCH	11	3208	3153
νCH	6	3202	3148
νCH	12	3197	3143
νCH	5	3196	3142
νCH	2	3186	3132
ν_{as}CH	11	3185	3131
ν_{as}CH	1	3179	3125
ν_{as}CH	4	3170	3116
ν_{as}CH	21	3150	3096
νCH	1	3145	3092
$\nu_{as}CH_3$ (OMe)	23	3137	3084
$\nu_{as}CH_3$ (OMe)	34	3069	3017
νCH_3 (OMe)	59	3008	2957
νC=O + νCC	158	1710	1681
νC=O + νCC+ ipb HCC	4	1655	1585
νC=O + νCC+ ipb HCC	394	1641	1572
νC=O + νCC+ ipb HCC	608	1625	1557
νCC+ ipb HCC	40	1618	1550
νCC+ ipb HCC	45	1601	1534
νCC+ ipb HCC	118	1543	1478
νCC + ipb HCC	62	1537	1472
δ CH_3 (OMe)	36	1503	1440
δ CH_3 (OMe)	9	1493	1430
CH_3umb.	2	1475	1413
ipb HCC + ipb COH	146	1464	1403
νCC + ipb HCC	36	1447	1386
νC-O + ipb HCC	163	1289	1235
νC-O + ipb HCC	277	1279	1225
ipb HCC + ipb COH	272	1229	1177
ω CH_2	14	1201	1151
ipb HCC + ipb COH	542	1185	1135
ρ CH_2	1	1167	1118
νC-O + ipb HCC	54	1060	1015
νC-O + Ph ring breathing	160	1034	991
ipb HCC	0	1024	981
opb HCC	1	970	929
Ph ring breathing	1	906	868
opb HCC	0	888	851
Ph breathing	27	848	812

Abbreviations; I_{IR}: IR intensity, ν: symmetricstretching, ν_{as}: asymmetricstretching, ipb: in planebending, opb: out of planebending, δ: scissoring, ω: wagging, ρ: rocking, umb: umbrella

311++G (d, p) basis set level in both gas and solvent environments. The investigation of such parameters is constructed on the values of enthalpy (ΔH), entropy (S), free energy (ΔG) and heat capacity (Cv), which are key concepts for understanding the thermodynamics of a substance[62]. Electronic, translational, rotational, and vibrational partition functions contribute to thermodynamic parameters. Since vibrational freedom provides the greatest contribution to the relevant quantities, $\Delta E_{vib.}$, $S_{vib.}$, and $Cv_{vib.}$parameters were also calculated[63]. Computed values are displayed in Table 4. Accordingly, ΔE, ΔH, and ΔG values for the gas phase were calculated as –843.737 a.u., –843.737 a.u., and –843.802 a.u., respectively. It is observed that the relevant values decrease in the acetonitrile, DMSO and water phases. In addition, the variations in $\Delta E_{thermal}$(kcal/mol), Cv (cal/molK), and S (cal/molK) values according to phases were computed as follows: $\Delta E_{thermal}$: 173.877 (gas) > 173.827 (acetonitrile) > 173.824 (DMSO) > 173.822 (water); Cv: 64.999 (gas) > 64.918 (water) >64.917 (acetonitrile & DMSO); S: 137.736 (gas) >137.077 (water) > 137.076 (acetonitrile & DMSO). Referring to Table 4, it is obvious that the contributions of vibrational freedom (namely, $\Delta E_{vib.}$, $Cv_{vib.}$, $S_{vib.}$) to $\Delta E_{thermal}$, Cv and S values are quite high. In the case of polarizability values (α, a.u.), the following values were obtained for each phase: 236.403 (gas) < 326.212 (acetonitrile) < 327.501(DMSO) < 329.197 (water). Based on this, the dielectric constant of the medium affects the polarizability value. The studied chalcone derivative is expected to be more polarizable in the water environment.

Table 4 — Thermodynamic and physicochemical parameter predictions for the title compound

	Gas	Acetonitrile	DMSO	Water
DM (Debye)	6.027	8.673	8.712	8.762
ΔE (a.u.)	–843.737	–843.754	–843.755	–843.755
ΔH (a.u.)	–843.737	–843.753	–843.754	–843.754
ΔG (a.u.)	–843.802	–843.819	–843.819	–843.819
$\Delta E_{thermal}$(kcal/mol)	173.877	173.827	173.824	173.822
$\Delta E_{vib.}$ (kcal/mol)	172.100	172.049	172.047	172.044
Cv (cal/molK)	64.999	64.917	64.917	64.918
$Cv_{vib.}$ (cal/molK)	59.037	58.955	58.956	58.956
S (cal/molK)	137.736	137.076	137.076	137.077
$S_{vib.}$ (cal/molK)	60.788	60.118	60.118	60.119
α (a.u.)	236.403	326.212	327.501	329.197

FMO and MEP analyses

The phenomenon of frontier molecular orbitals, which is frequently encountered in computational chemistry, involves examining both the energies and electron density distributions of HOMOs and LUMOs. Analyzing this phenomenon allows the prediction of some quantities such as energy gap, chemical hardness, electronegativity. This information ensures insights into the stability and reactivity of the molecule of interest[64-66]. In this part of the study, some quantum chemical reactivity parameters were calculated for the title compound at the level of theory under study, in accordance with the relevant equations (6)-(13). The alterations of the relevant parameters according to the dielectric

constant of the medium were perused. The data obtained are presented in Table 5. Accordingly, while the energy gap ($\Delta E = E_{LUMO}-E_{HOMO}$) values for acetonitrile, DMSO, and water phases were found to be 3.753, 3.750, and 3.747 eV, respectively, a higher energy gap value of 3.940 eV was determined in the gas phase. The following ranking was obtained for chemical hardness values displaying a similar trend: η in eV; 1.970 (gas) > 1.877 (acetonitrile) > 1.875 (DMSO) > 1.874 (water). Chemical hardness and energy gap values are directly proportional to each other and inversely proportional to the reactivity of the molecule. A small ΔE value (small chemical hardness) indicates high reactivity and low stability. It also shows up remarkable likelihoods of intramolecular charge transfer, hence higher polarizability. On the other side, molecules with large ΔE values (large chemical hardness) are less polarizable molecules with lower reactivity and are referred to as hard molecules[67]. From the outcome of the computations, it was determined that the electrophilicity index value of the gas phase was relatively lower than that of the solvent phases. The order of relevant values is as follows: ω in eV; 5.086 (water) > 5.074 (DMSO) > 5.064 (Acetonitrile) > 4.490 (gas). On account of this, the title compound is expected to exhibit slightly more electrophilic character in aqueous environment.

Table 5 — The calculated quantum chemical reactivity parameters of the title compound

	Gas	Acetonitrile	DMSO	Water
E_{HOMO}	–6.176	–6.236	–6.237	–6.239
E_{LUMO}	–2.236	–2.483	–2.487	–2.492
ΔE	3.940	3.753	3.750	3.747
η	1.970	1.877	1.875	1.874
μ	–4.206	–4.360	–4.362	–4.366
χ	4.206	4.360	4.362	4.366
ω	4.490	5.064	5.074	5.086
ω^+	2.633	3.119	3.127	3.138
ω^-	6.839	7.478	7.489	7.503
ΔN_{max}	2.135	2.323	2.326	2.330
ΔE_{back}	–0.493	–0.469	–0.469	–0.468

The pictorial presentation of the HOMO and LUMO densities and DOS diagram of studied chalcone derivative is introduced in Fig. 3. The red and green colours designate negative and positive lobes, respectively. With respect to Fig. 3, it is clearly seen that HOMO and LUMO densities are distributed almost throughout the molecule. Besides, Fig. 4 represents the MEP and ESP maps created using B3LYP/6-311++G (d, p) theory level for the title compound. Isodensity valuation is 0.0004 a.u. The molecular electrostatic potential surface mapping is extremely useful for defining feasible electrophilic and nucleophilic attack sites. It is specified utilizing the total charge density, involving both the electrons and protons of the studied molecule. In this method, which uses color regulations, red designates the most negative electrostatic potential and blue designates the

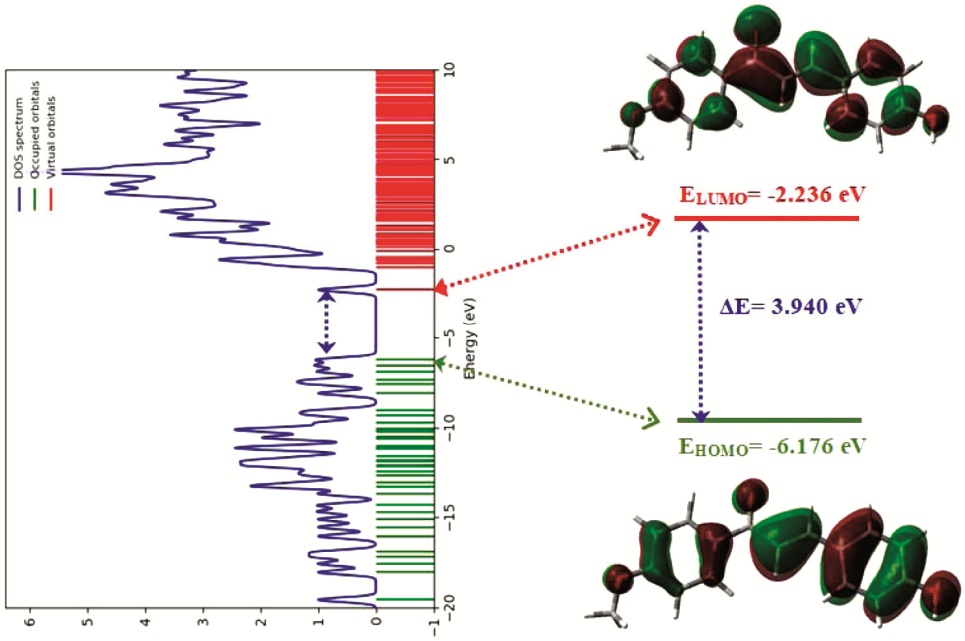

Fig. 3 — DOS plot and HOMO & LUMO surfaces (isoval: 0.02 a.u.) of the title compound

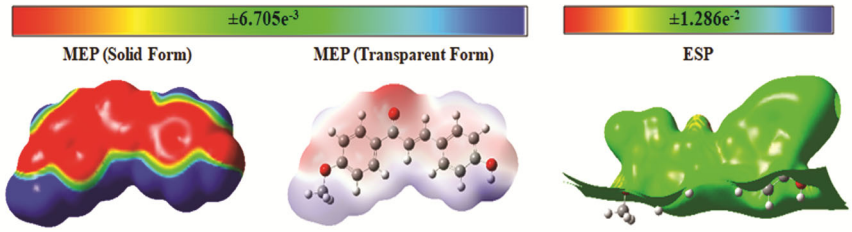

Fig. 4 — MEP & ESP surfaces created using B3LYP/6-311++G (d, p) theory level

Table 6 — Theoretical UV-Vis absorption characteristics of the title compound

Medium	ES	$\lambda_{calc.}$ (nm)	ΔE (eV)	*f*	Symmetry	Major Contributions
Water	S_1	365	3.3981	1.0207	Singlet-A	H→L (69%)
	S_2	354	3.5014	0.0033	Singlet-A	H-2→L (68%)
	S_3	319	3.8791	0.0823	Singlet-A	H-1→L (67%)
	S_4	286	4.3314	0.0029	Singlet-A	H-3→L (62%), H-4→L (23%)
	S_5	285	4.3412	0.0035	Singlet-A	H-4→L (57%), H→L+2 (26%)
	S_6	259	4.7721	0.0683	Singlet-A	H→L+1 (65%), H-4→L (23%)
Acetonitrile	S_1	364	3.3996	1.0219	Singlet-A	H→L (69%)
	S_2	354	3.4964	0.0034	Singlet-A	H-2→L (68%)
	S_3	320	3.8795	0.0826	Singlet-A	H-1→L (67%)
	S_4	286	4.3338	0.0030	Singlet-A	H-3→L (63%), H-4→L (20%)
	S_5	285	4.3446	0.0033	Singlet-A	H-4→L (58%), H→L+2 (26%)
	S_6	260	4.7718	0.0683	Singlet-A	H→L+1 (65%), H-4→L (23%)
DMSO	S_1	366	3.3846	1.0377	Singlet-A	H→L (69%)
	S_2	354	3.4981	0.0034	Singlet-A	H-2→L (68%)
	S_3	320	3.8719	0.0867	Singlet-A	H-1→L (67%)
	S_4	286	4.3321	0.0032	Singlet-A	H-3→L (63%), H-4→L (21%)
	S_5	285	4.3425	0.0035	Singlet-A	H-4→L (58%), H→L+2 (26%)
	S_6	260	4.7683	0.0710	Singlet-A	H→L+1 (65%), H-4→L (23%)

H = HOMO; L = LUMO

most positive electrostatic potential[68,69]. The molecular electrostatic potential of title compound was calculated in the range of –0.006705 a.u (deepest red) – +0.006705 a.u. (deepest blue). Also, ESP map was colored from deepest red (–0.01286 a.u.) to deepest blue (0.01286 a.u.). Consequently, it can be pointed out that the electron density is higher around O1, O2, and O3 atoms and there is predominantly red coloration. On the other hand, due to the low electron density, blue coloration is mostly noticeable around hydrogen atoms.

UV-Vis characterization

The excited state properties of the title compound in water, acetonitrile, and DMSO environments were calculated by TD-DFT method based on the optimized ground state geometry. The IEFPCM model was used to compare the solvent effects on UV-vis absorption characteristics. The outcomes revealed by calculations are presented in detail in Table 6. From Table 6, it is observed that the values of absorption peaks and transition types are not crucially affected by the solvent environment. The transition type with the highest oscillator strength (*f*; 1.0207, 1.0219, and 1.0377) for the water, acetonitrile, and DMSO phases is the S_1 singlet state. As can be evident from the TD-DFT, the absorption wavelength (λ_{calc}) values corresponding to this transition were calculated as 365 ,364, and 366 nm. It was determined that the mentioned UV-vis absorption maxima correspond to the electron transition from HOMO to LUMO. To gain more insights into the molecular orbitals contributing to the transitions identified for the DMSO phase, their spatial distributions are picturized and exhibited in Fig. 5. Accordingly, whole absorption wavelengths can be qualified as π→π* and n→π* transition type.

NBO analysis

Quantum chemical examination of charge transfer interactions from donor orbitals to acceptor ones is performed with the help of NBO analysis. In this section, the title compound was subjected to NBO analysis using the B3LYP hybrid functional and the 6-311++G (d, p) basis set in gas phase. By applying 2nd-order perturbation theory, probable donor-acceptor interactions and their corresponding

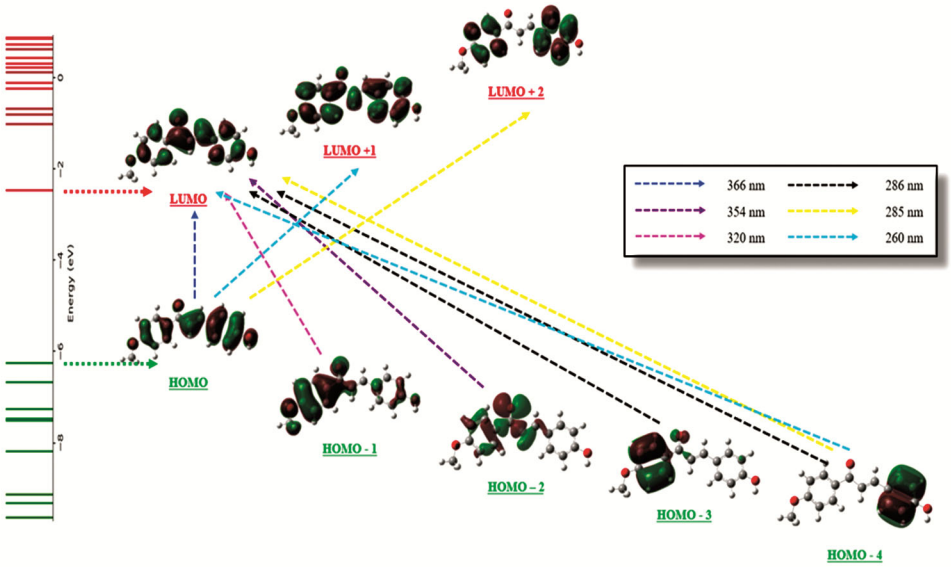

Fig. 5 — FMO diagrams contributing to the electronic transitions identified for DMSO phase

Table 7 — NBO analysis results of the possible interactions for the title molecule

Donor(i)	ED_i/e	Acceptor(j)	ED_j/e	$E^{(2)}$ kcal/mol	E(j)-E(i)/a.u	F(i.j)/a.u
π C4-C10	1.84219	π* O1-C5	0.22418	20.57	0.30	0.071
		π* C6-C17	0.39544	11.44	0.29	0.055
π C6-C17	1.61316	π* C4-C10	0.11891	17.95	0.29	0.070
		π* C8-C12	0.38181	19.07	0.27	0.064
		π* C23-C25	0.31979	22.68	0.27	0.071
π C7-C15	1.65593	π* O1-C5	0.22418	19.26	0.28	0.068
		π* C11-C19	0.38743	16.82	0.27	0.061
		π* C13-C21	0.26617	20.27	0.29	0.070
π C8-C12	1.61632	π* C6-C17	0.39544	24.09	0.29	0.075
		π* C23-C25	0.31979	16.82	0.28	0.063
π C11-C19	1.65088	π* C7-C15	0.37065	23.42	0.30	0.075
		π* C13-C21	0.26617	14.00	0.30	0.059
π C13-C21	1.70031	π* C7-C15	0.37065	16.35	0.28	0.062
		π* C11-C19	0.38743	23.43	0.27	0.073
π C23-C25	1.71853	π* C6-C17	0.39544	15.47	0.29	0.062
		π* C8-C12	0.38181	22.09	0.28	0.072
LP (2) O1	1.88873	σ* C5-C7	0.06499	19.86	0.65	0.102
		σ* C5-C10	0.05813	19.85	0.66	0.103
LP (2) O2	1.83139	π* C11-C19	0.38743	37.93	0.28	0.098
LP (2) O3	1.86929	π* C8-C12	0.38181	27.34	0.35	0.094

stabilization energy values ($E^{(2)}$)were calculated. The outputs obtained as a result of the analysis are listed in Table 7. Stabilization energy values of 10 kcal/mol and above were taken into account. Table 7 reflects the information that the possible interaction types are π → π*, LP → σ* and LP → π*. While the total stabilization energy value resulting from π-π* interactions was calculated as 303.73 kcal/mol, the total value for LP-π* interactions was found to be 65.27 kcal/mol. Among the π-π* interactions with energy values ranging from 11.44 kcal/mol to 24.09 kcal/mol, the maximum contributor is the electron donation from π C8-C12 (ED_i =1.61632e) to the π* C6-C17 (ED_j= 0.39544e) with a stabilization energy of 24.09 kcal/mol. On the other hand, the highest stabilization energy values were calculated as 37.93 kcal/mol and 27.34 kcal/mol, and correspond to LP (2) O2 (ED_i =1.83139e) → π* C11-C19 (ED_j = 0.38743e) and LP (2) O3 (ED_i = 1.86929e) → π* C8-C12 (ED_j = 0.38181e) transitions, respectively. For the LP (2) O1→ σ* C5-C7 and LP (2) O1→ σ* C5-C10 transitions, very close energy values were calculated as 19.86 and 19.85 kcal/mol.

In silico ADME predictions

The development of effective and safe bioactive drug precursors is a multi-step, time-consuming and financially burdensome process. In order to make this process more qualified in every respect, researchers have turned to *in silico* methods in the light of advances in computational techniques and computer hardware. In this context, the field of cheminformatics, which systematizes computer applications in chemistry, facilitates the development of new compounds and methods for chemists. Cheminformatics has many applications in the discovery and optimization of new lead compounds, determination of quantitative structure-activity relationships, analysis of data from high-throughput screening methods, and modelling of ADME-Tox data[70,71]. The sum of the events that occur from the intake of a chemical into the biological system to its excretion is called ADME. It refers to absorption, distribution, metabolism and excretion, respectively. In the case of ADME characteristics of a drug-like molecule are of sufficiently high quality, the molecule could be evaluated for a next step. Therefore, in this section, the title compound is subjected to *in silico* evaluations. SwissADME web server[37] was utilized for this purpose. First, the SMILES (**S**implified **M**olecular **I**nput **L**ine **E**ntry **S**pecification, COC1=CC=C(C=C1)C(=O)\C=C\C1=CC=C(O)C=C1) string of the studied chalcone derivative was created and uploaded to the web platform. The parameters of interest of the questioned compound were accessed under the headings of physicochemical properties, pharmacokinetics, drug-likeness, lipophilicity, water solubility, and medicinal chemistry. The findings obtained are presented in Table 8. Under the heading of physicochemical properties; values of parameters such as molecular weight, Csp3 fraction, number of rotatable bonds, number of H-bond acceptors and donors, and topological polar surface area (TPSA) were calculated. Table 8 contains data on gastrointestinal (GI) absorption, blood-brain barrier (BBB) permeability, *P*-gp substrate, inhibition of CYP enzymes, and skin permeability ($logK_p$) as pharmacokinetic properties. Blood-brain penetration (BBB) and gastrointestinal absorption (GI) features were scrutinized using the BOILED-Egg (**B**rain **O**r **I**ntestina**LE**stimate**D** absorption) method. The BOILED-Egg graph of the studied compound is shown in Fig. 6(b). Accordingly, in the graph, it can be seen that the title compound is located in the yellow region

Table 8 — Key parameters of *in silico* analysis of the title compound

Physicochemical properties		Pharmacokinetics	
Formula	C16H14O3	GI absorption	High
Molecular weight (g/mol)	254.28	BBB permeant	Yes
Num. heavy atoms	19	*P*-gp substrate	No
Num. arom. heavy atoms	12	CYP1A2 inhibitor	Yes
Fraction Csp3	0.06	CYP2C19 inhibitor	Yes
Num. rotatable bonds	4	CYP2C9 inhibitor	Yes
Num. H-bond acceptors	3	CYP2D6 inhibitor	No
Num. H-bond donors	1	CYP3A4 inhibitor	Yes
Molar Refractivity	74.76	Log K_p (skin permeation)	–5.33 cm/s
TPSA (Å²)	46.53		
Lipophilicity		Druglikeness	
Log $P_{o/w}$ (iLOGP)	2.47	Lipinski	Yes; 0 violation
Log $P_{o/w}$ (XLOGP3)	3.55	Ghose	Yes
Log $P_{o/w}$ (WLOGP)	3.19	Veber	Yes
Log $P_{o/w}$ (MLOGP)	2.42	Egan	Yes
Log $P_{o/w}$ (SILICOS-IT)	3.48	Muegge	Yes
Consensus Log $P_{o/w}$	3.02	Bioavailability Score	0.55
WaterSolubility		Medicinal Chemistry	
Log S (ESOL)	–3.86	PAINS	0 alert
Solubility (mg/mL)x10^{-2}	3.54	Brenk	1 alert: michael_acceptor_1
Class	Soluble	Leadlikeness	No; 1 violation: XLOGP3>3.5
Log S (Ali)	–4.21	Synthetic accessibility	2.40
Solubility (mg/mL)x10^{-2}	1.56		
Class	Moderately soluble		
Log S (SILICOS-IT)	–4.51		
Solubility (mg/mL)x10^{-3}	7.86		
Class	Moderately soluble		

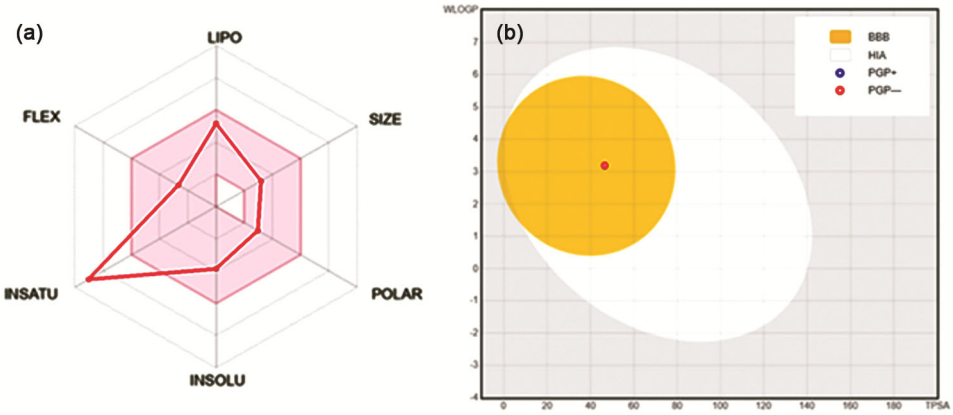

Fig. 6 — Bioavailability radar (a); BOILED-Egg diagrams (b): BBB (Blood-Brain Barrier) yellow yolk-like sphere, HIA (Human Intestinal Absorption) oval white part, PGP+ *P*-glycoprotein substrate, PGP- a non-*P*-glycoprotein substrate.

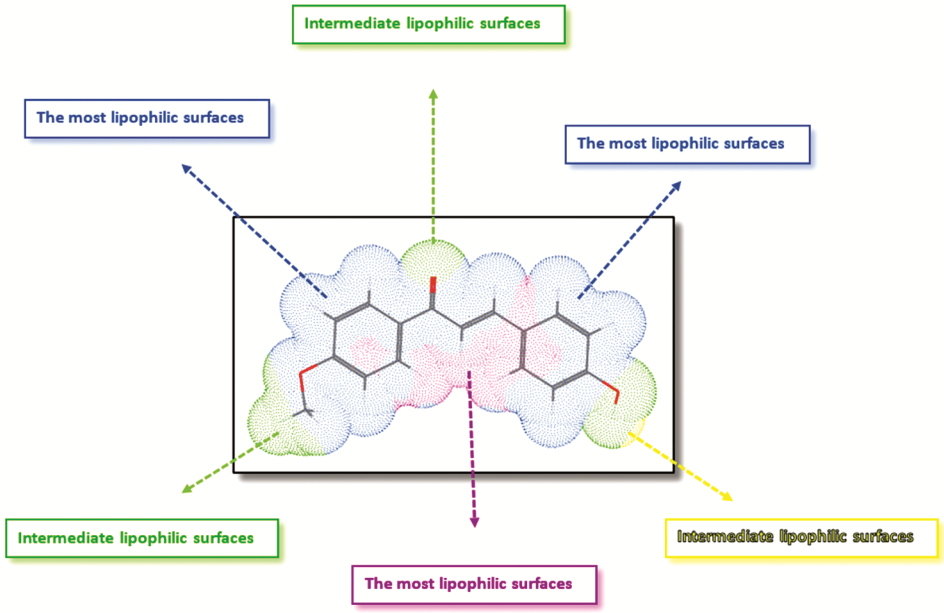

Fig. 7 — Molecular lipophilicity potential (MLP) map of the title compound

as a red hollow sphere. Based on the data in Table 8, regarding Cytochrome P450 (CYP) inhibitors, it can be said that the title compound present inhibition properties for CYP1A2, CYP2C19, CYP2C9, and CYP3A4, excluding CYP2D6. Considering the bioavailability radar diagram (Fig. 6(a)), the pink-colored zone represents the physicochemical area suitable for oral bioavailability[72]. It was established that the physicochemical characteristics of the examined derivative were within the boundaries determined by the pink zone, except for insaturation. Also, bioavailability score was predicted as 0.55.

Under the title of lipophilicity, $logP_{o/w}$ (partition coefficient between n-octanol and water) values of the molecule of interest were calculated according to five different methods (iLOGP, XLOGP3, WLOGP, MLOGP, and SILICOS-IT). Consensus values represent the average lipophilicity value. Lipophilicity is an important factor regarding permeability through biological membranes. From Table 7, the Consensus log Po/w value was calculated as 3.02. In addition, lipophilicity assessments can be enhanced using visualization methods.Towards this end, a molecular lipophilicity potential (MLP) map (Fig. 7) was created for the title compound *via* Molinspiration web server[43, 44] and lipophilic interaction regions were determined.As can be clearly seen from Fig. 7, the regions where purple and blue colours are dominant

represent the surfaces where lipophilic interactions are most intense, while the yellow and green regions represent intermediate lipophilic interactions. Therefore, it is concluded that aromatic rings in the title compound promote lipophilic interactions.

Conclusions

This current study was mainly conceived to explore thermodynamic, electronic, physicochemical, and ADME characteristics of the title compound from theoretical aspects.The main findings can be summarized as follows: 1) It was determined that the theoretical bond parameters and vibrational analysis results were consistent with the experimental data. 2) For the gas phase, ΔE, ΔH, and ΔG values were calculated as –843.737, –843.737 and –843.802 a.u., respectively, while it was observed that the relevant values decreased in the solvent phases. 3) Energy gap (ΔE) is considered an important metric of stability.The highest energy gap value was calculated as 3.940 eV in the gas phase. Relatively lower values were obtained for the solvent phases. 4) *In silico* analysis results indicate that the physicochemical properties of the examined derivative are within the determined limits, except for unsaturation. Additionally, the bioavailability score was estimated at 55%. 5) The lipophilic character of the title compound was examined both numerically (consensus $\log P_{o/w} = 3.02$) and visually (MLP map).It is prominent that the results support each other.

As pointed out earlier, members of the chalcone family are proven candidates for potential applications in different disciplines.It is expected that the findings revealed in the study will help find effective application areas by providing detailed perspectives for further research.

Acknowledgement

The numerical calculations reported in this paper were partially performed at TUBITAK ULAKBIM, High Performance and Grid Computing Centre (TRUBA resources).

References

1 Narwal S, Devi B, Dhanda T, Kumar S & Tahlan S, *J Mol Struc*, 1303 (2024) 137554.
2 Narwal S, Kumar S & Verma P K, *Res Chem Intermed*, 47 (2021) 1625.
3 Yadav P, Lal K, Kumar A, Guru S K, Jaglan S & Bhushan S, *Eur J Med Chem,* 126 (2017) 944.
4 Bonesi M, Loizzo M R, Statti G A, Michel S, Tillequin F & Menichini F, *Biorg Med Chem Lett,*20 (2010) 1990.
5 Wang G, Xue Y, An L, Zheng Y, Dou, Y, Zhang L & Liu Y, *Food Chem,* 171 (2015) 89.
6 Reddy M V B, Hung H Y, Kuo P C, Huang G J, Chan Y Y, Huang S C, Wu S J, Morris-Natschke S L, Lee K H & Wu T S, *Bioorg Med Chem Lett,*27 (2017)1547.
7 Bhale P S, Chavan H V, Dongare S B, Shringare, S N, Mule Y B, Nagane S S & Bandgar B P, *Bioorg Med Chem Lett,* 27 (2017) 1502.
8 Sharma C S, Shekhawat K S, Chauhan C S & Kumar N, *J Chem Pharm Res,* 5 (2013) 450.
9 Konduru N K, Dey S, Sajid M, Owais M & Ahmed N, *Eur J Med Chem*, 59 (2013) 23.
10 Parikh K & Joshi D, *Med Chem Res,* 22 (2013) 3688.
11 Mahesha P, Shetty N S & Kulkarni S D, *J Fluoresc,* 32 (2022) 835.
12 Lim K E S, Ang K Y D, Chong Z X, Lim Y Z, Lin Q, Wang Y, Lee P P F, Ganguly R & Tan Y L K, *Inorganica Chim Acta*, 565 (2024) 121963.
13 Vasudha D, Jagadeesh A, Konidala S K, Yasin H, Mali S N, Bhandare R R & Shaik A B, *Chem Phy Imp,* 8 (2024) 100472.
14 Bandaru V, Juvale K, Anugu S R, Vishwakarma S, Kumar A, Doddipalla R, Kumari K S, Jadhav V & Vidavalur S, *J Mol Struct*, 1309 (2024) 138149.
15 Kawale R A, Akolkar H N, Shaikh M H, Khedkar V M, Raut D N, Darekar N R, Wable J B & Shelke S N, *Polycycl Aromat Comp*, (2023) 1.
16 Nair A R, Raksha C, Heera R, Mohan M G, Manoj P & Sivan A, *J Photochem Photobio, A*451 (2024) 115511.
17 Hassan A F, Hussein O, Al-Barazenji, T, Allouch A, Kamareddine L, Malki A, Al Moustafa A & Khalil A, *Heliyon,* 10 (2024) 27002.
18 Nanjundaswamy S, Shanthakumar K C, Shadakshari, S, Rajabathar J R, Arokiyaraj S, Al-lohedan H A, Sakthipandi K & Mallu P, *ACS Omega,* 9 (2024) 13603.
19 Zhang N, Zeng W, Zhou Q, Sun Z, Meng K, Qin Y, Hu Y & Xue W, *Arabian J Chem,* 17 (2024) 105368.
20 Sadineni K, Basireddy S R, Allaka T R, Yatam S, Bhoomandla S, Muvvala V & Haridasyam S B, *Chem Biodivers*, (2024) 202400389.
21 Zhuang C, Zhang W, Sheng C, Zhang W, Xing C & Miao Z, *Chem Rev*, 117 (2017) 7762.
22 Qiu X Y, Yang S L, Liu W S & Zhu H L, *Acta Cryst,* E62 (2006) 3324.
23 Wilhelm A, Bonnet S L, Twigge L, Rarova L, Stenclova T, Visser H G & Schutte-Smith M, *J Mol Struct,* 1251 (2022) 132001.
24 Frisch M J, Trucks G W, Schlegel H B, Scuseria G E, Robb M A, Cheeseman J R, Scalmani G, Barone V, Petersson G A, Nakatsuji H, Li X, Caricato M, Marenich A V, Bloino J, Janesko B G, Gomperts R, Mennucci B, Hratchian H P, Ortiz J V, Izmaylov A F, Sonnenberg J L, Williams Young D, Ding F, Lipparini F, Egidi F, Goings J, Peng B, Petrone A, Henderson T, Ranasinghe D, Zakrzewski V. G, Gao J, Rega N, Zheng G, Liang W, Hada M, Ehara M, Toyota K, Fukuda R, Hasegawa J, Ishida M, Nakajima T, Honda Y, Kitao O, Nakai H, Vreven T, Throssell K, Montgomery J A Jr, Peralta J E, Ogliaro F, Bearpark M J, Heyd J J, Brothers E N, Kudin K N, Staroverov V N, Keith T A, Kobayashi R, Normand J, Raghavachari K, Rendell A P, Burant J C,

Iyengar S S, Tomasi J, Cossi M, Millam J M, Klene M, Adamo C, Cammi R, Ochterski J W, Martin R L, Morokuma K, Farkas O, Foresman J B & Fox D J, *Gaussian 16* Rev. C.01, (Wallingford, CT) 2016.
25 Lee C, Yang W & Parr R G, *Phys Rev B,* 37 (1988) 785.
26 Becke A D, *J Chem Phys,* 98 (1993) 1372.
27 Becke A D, *J Chem Phys,* 98 (1993) 5648.
28 Dennington R, Keith T A & Millam J M, *Gauss View*, Version 6, (Semichem Inc., Shawnee Mission, K S) 2016.
29 O'Boyle N M, Tenderholt A L & Langer K M, *J Comp Chem*, 29 (2008) 839.
30 Tomasi J, Mennucci B & Cammi R, *Chem Rev,* 105 (2005) 2999.
31 Tomasi J, Mennucci B & Cance`s E, *J Mol Struct (Theochem),*464 (1999) 211.
32 Casida M E, Jamorski C, Casida K C & Salahub D R, *J Chem Phys,* 108 (1998) 4439.
33 Scalmani G, Frisch M J, Mennucci B, Tomasi J, Cammi R & Barone V, *J Chem Phys,*124 (2006) 1.
34 Van Caillie C & Amos R D, *Chem Phys Lett,* 308 (1999) 249.
35 Adamo C & Jacquemin D, *Chem Soc Rev,* 42 (2013) 845.
36 Importa R, Ferrante C, Bozioc R & Barone V, *Phys Chem Chem Phys*, 11 (2009) 4664.
37 Daina A, Michielin O & Zoete V, *Sci. Rep.*7 (2017) 42717.
38 Cheng T, Zhao Y, Li X, Lin F, Xu Y, Zhang X, Li Y & Wang R, *J Chem Inf Model,* 47 (2007) 2140.
39 Daina A, Michielin O & Zoete V, *J Chem Inf Model,* 54 (2014) 3284.
40 Wildman S A & Crippen G M, *J Chem Inf Comput Sci,* 39 (1999) 868.
41 Lipinski C A, Lombardo F, Dominy B W & Feeney P J, *Adv Drug Deliv Rev,* 46 (2001) 3.
42 Silicos-it. (n.d.). Retrieved from https://www.silicos-it.be.
43 Molinspiration Cheminformatics free web services, https://www.molinspiration.com, Slovensky Grob, Slovakia.
44 Gaillard P, Carrupt P A, Testa B & Boudon A, *J Comput Aided Mol Des*, 8 (1994) 83.
45 McQuarrie D A, *Statistical Thermodynamics*, (Harper & Row Publishers, New York), 1973.
46 Hill T L, *An Introduction to Statistical Thermodynamics*, (Addison- Wesley Publishing, Inc, London) 1962.
47 Herzberg G, *Molecular Spectra and Molecular Structure III*, 1st Edition, (D Van Nostrand Company, Inc., New York) 1964.
48 Serdaroğlu G, Durmaz S, *Indian J Chem,* 49 (2010) 861.
49 Koopmans T, *Physica,* 104 (1934) 1.
50 Parr R G, Szentpaly L V & Liu S, *J Am Chem Soc,* 121 (1999) 1922.
51 Parr R G & Pearson R G, *J Am Chem Soc,* 105 (1983) 7512.
52 Pearson R G, *Proc Natl Acad Sci U S A,* 83 (1986) 8440.
53 Perdew J P & Levy M, *Phys Rev Let,* 51 (1983) 1884.
54 Perdew J P, Parr R G, Levy M & Balduz J L, *Phys Rev Let,* 49 (1982).
55 Gazquez J L, Cedillo A & Vela A, *J Phys Chem A,* 111 (2007) 1966.
56 Gomez B, Likhanova N V, Domínguez-Aguilar M A, Martínez-Palou R, Vela A & Gazquez J L, *J Phys Chem B,* 110 (2006) 8928.
57 Weinhold F, Landis C R & Glendening E D, *Int Rev Phys Chem,* 35 (2016) 399.
58 Reed A E, Curtiss L A & Weinhold F, *Chem Rev,* 88 (1988) 899.
59 Sundaraganesan N, Ilakiamani S, Salem H, Wojciechowski P M & Michalska D, *Spectrochim Acta A Mol Biomol Spectrosc,* 61 (2005) 2995.
60 Arı H, Özpozan T, Büyükmumcu Z, Akın N & İlhan İ Ö, *J Mol Struct,* 1250 (2022) 131820.
61 Smith B, *Infrared Spectral Interpretation, A Systematic Approach*, (CRC Press, Washington, DC) 1999.
62 Rahman S, Hussain A, Noreen S, Bibi N, Arshad S, Rehman J U & Tahir M B, *J Solid State Chem,* 317 (2023) 123650.
63 Serdaroğlu G, Uludağ N, Sugumar P & Rajkumar P, *J Mol Struct,* 1244 (2021) 130978.
64 Serdaroğlu G, Uludağ N & Üstün E, *Chem Sel,* 9 (2024) 202303222.
65 Serdaroğlu G, Uludağ N & Üstün E, *Chem Sel*, 9 (2024) 202400019.
66 Shafiq I, Amanat I, Khalid M, Asghar M A, Baby R, Ahmed S & Alshehri S M, *Syn Met,* 297 (2023) 117410.
67 Khalid M, Ullah M A, Adeel M, Khan M U, Tahir M N & Braga A A C, *J Saudi Chem Soc,* 23 (2019) 546.
68 Murray J S & Politzer P, *Wiley Interdisc Rev Comp Mol Sci,* 1 (2011) 153.
69 Murray J S & Sen K, *Molecular Electrostatic Potentials: Concepts and Applications,* first ed., (Elsevier, Amsterdam) 1996.
70 Zadorozhnii P V, Kiselev V V & Kharchenko A V, *Fut Pharm,* 2 (2022) 160.
71 Durán-Iturbide N A, Díaz-Eufracio B I & Medina-Franco J L, *ACS Omega*, 5 (2020) 16076.
72 Ahmad I, Khan H & Serdaroglu G, *Comp Biol Chem*, 104 (2023) 107861.